17th World Conference on Earthquake Engineering, 17WCEE
Sendai, Japan - September 13th to 18th 2020

EXPERIMENTAL INVESTIGATION OF HOLLOW PRECAST STEEL-ENCASED CONCRETE PILES

S. Thusoo[(1)], S. Kono[(2)], J. Hamada[(3)], Y. Asai[(4)], D. Mukai[(5)]

[(1)] *Graduate Student, Dept. of Civil and Environmental Engineering, Tokyo Institute of Technology, thusoo.s.aa@m.titech.ac.jp*
[(2)] *Professor, Institute of Innovative Research, Tokyo Institute of Technology, kono.s.ae@m.titech.ac.jp*
[(3)] *Chief Researcher, Research Development Institute, Takenaka Corporation, hamada.junji@takenaka.co.jp*
[(4)] *Dr. Eng., Concrete Pile Installation Technology Association, yoitiasai@toyoasano.co.jp*
[(5)] *Associate Professor, Dept. of Civil and Architectural Engineering, University of Wyoming, dmukai@uwyo.edu*

Abstract

Steel-encased concrete (SC) piles, when used near a pile cap, increase the moment and shear capacities of the pile-pile cap connection, as compared to using prestressed high-strength concrete (PHC) or prestressed reinforced concrete (PRC) piles. Hence, SC piles are frequently used in Japan for the development of earthquake-resistant pile systems. These piles are mainly designed for levels of low-moderate seismicity and the guidelines for the design of these piles in levels of high seismicity have not been established yet. Also, with the increasing commercial use of SC piles for bridge and building constructions it is crucial to bring the current seismic design guidelines for these piles in line with the codes for superstructure elements regarding the performance at ultimate and safety states. Hence, there is an imminent need for the development of a performance-based design framework targeted for SC piles.

For this work flexure tests were conducted on 7 prefabricated SC piles of diameter 400 mm and length 1.2 m under different conditions of axial load ratio (0~0.35), steel casing thickness (4.5~6.0 mm), concrete layer thickness (50~68 mm) and core filling (hollow, cement paste filled, normal concrete filled). To understand the flexural behavior of tested piles, the observed failure modes, and influence of concrete crushing and local buckling of steel casing on moment carrying capacity were examined in detail while paying attention to the post-peak behavior. The moment-curvature relation of tested piles was evaluated theoretically using bilinear concrete and steel models which were based on the 2017 AIJ guidelines for seismic design of reinforced concrete foundation members (draft). The evaluation showed that the theoretical strength calculations for both maximum and ultimate capacities became unreliable in cases with high axial load ratios because buckling preceeded the occurrence of theoretical maximum strength. The authors established lower and upper bound models, based on an improved concrete model for high-strength concrete and degree of concrete confinement, to predict the maximum moment capacities. It was observed that the upper and lower bound models were able to bracket the moment capacities from tests for SC piles under all levels of axial loads.

The results from this study are valuable and useful for engineers designing foundations in seismic areas. In particular, this study helps engineers to determine the moment capacity of SC piles and understand the flexural behavior of SC piles up to the ultimate state.

Keywords: Buckling of steel; High-strength concrete; Hollow spun pile; Performance evaluation; Precast pile

1. Introduction

Several failures in piles supporting buildings were observed after the Hyogoken-Nambu earthquake in 1995. These damages occurred due to the failure of piles in the bending shear mode and subsequent crushing of the weakened sections. The reconnaissance surveys held in the Kobe area after this earthquake **[1,2]** reported that the piles used were mostly precast, prestressed concrete piles constructed before the 1980s and precast, prestressed high strength concrete (PHC) piles constructed afterward. An important observation from this investigation was that at sites where PHC piles were joined with steel pipe reinforced concrete piles near the head, little to no damage was observed even when liquefaction of under-laying soil layers had occurred.

At present, the commercial use of precast SC piles near pile heads for building constructions in Japan is increasing at a tremendous rate with each passing year. However, the guidelines for these piles use basic design models as the related researches are few. The pile manufacturers in Japan provide data regarding the allowable load capacity of precast SC piles, but there is very little data available to assess their ultimate flexural performance for seismic design.

The current study is prompted to understand the structural performance and hysteretic behavior of SC piles to improve the design guidelines and contribute to the ongoing development of Earthquake Resistant (ER) piles. To this end, the objective of this study is to accumulate and analyze data obtained from full-scale experiments on precast hollow steel-encased high-strength spun concrete piles tested under cyclic loading and to reproduce performance up to the ultimate load condition with a simple numerical analysis.

2. Outline of tests

2.1. Specimens

This paper reports the tests on seven steel-encased concrete (SC) piles with a diameter, D= 400 mm, shear span ratio = 3, and length, L= 1.2 m, tested in a cantilevered configuration under combined axial and bending loads. **Figure 1** shows the general cross-section of the specimens, and the specification for each manufactured unit is given in **Table 1**. Here, the axial load ratio, η, is the ratio of external applied axial load to the pure axial load carrying capacity based on the unfactored strengths of concrete, steel, and the filling areas. All specimens were tested under constant compressive axial loads with the ratio η varying from 0.00 to 0.35. All specimens were designed to fail in flexure and had a shear span to outer diameter ratio of 3.0. The mechanical properties of concrete, steel and filling material measured during material tests are shown in **Table 1**.

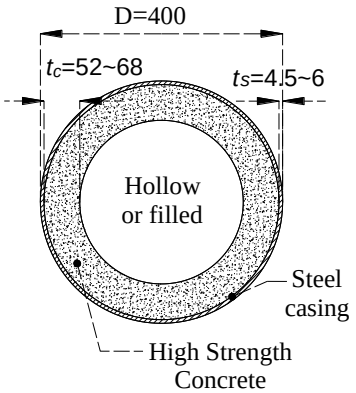

Figure 1: General cross-section of SC piles

The test variables were set as axial load ratio, η, steel to concrete strength ratio, $f_y A_s / f_c A_c$, properties of the core filling material and the presence or absence of a filled core. In the case of SC1, SC4 and SC 5, η was varied from 0.0 to 0.26, keeping all other variables the same. Steel to concrete strength was varied between SC7 and SC4 piles to study the effect of reducing the steel section. The hollow cores of SC8 and SC9 piles were filled with cement paste and normal concrete, respectively, to study the changes in failure mode and pile capacities caused by preventing the spalling of the inner face of concrete using low-cost materials. Additionally, the SC6 pile had a design thickness of 50 mm (for other piles, thickness was 65 mm) to study the effect of reducing the concrete section on pile capacities.

Table 1: Specimen properties and material specifications

Pile	D	$\frac{t_c}{D}$	$\frac{t_s}{D}$	N	η	f_c	E_c	f_y	E_s	f_{cf}	E_{cf}	Comment
	(mm)			(kN)		(MPa)	(GPa)	(MPa)	(GPa)	(MPa)	(GPa)	
SC1	400	0.17	0.015	0	0.00	115	45.6	505	212	-	-	Hollow
SC4	400	0.16	0.015	2000	0.18	111	44.2	505	212	-	-	Hollow
SC5	400	0.17	0.015	3000	0.26	115	45.6	505	212	-	-	Hollow
SC6	400	0.13	0.015	3500	0.35	115	45.6	505	212	-	-	Hollow
SC7	400	0.16	0.011	2000	0.20	115	45.6	453	207	-	-	Hollow
SC8	400	0.17	0.015	3500	0.27	122	46.7	408	201	27.4	9.95	Cement fill
SC9	400	0.17	0.015	3500	0.28	122	46.7	408	201	23.7	26.7	Concrete fill

D: Diameter of the pile; t_c: Thickness of concrete layer; t_s: Thickness of Steel layer; N: Applied axial load; η: Axial load ratio; f_c, f_{cf}: Compressive strength of concrete and filling, respectively; f_y: Yield strength of steel; E_c, E_s, E_{cf}: Young's modulus of concrete, steel, and filling, respectively.

2.2. Loading setup and instrumentation

The piles were tested as cantilevers with constant axial and reversed quasi-static cyclic lateral loads applied with displacement control in the lateral direction at the free end. **Figure 3** shows the schematics of the large-scale loading setup along with the simplified diagram of deformations and rotations measured at various heights of the specimen. The interaction of pile with soil was not considered here. This test setup allows the study of pile behavior with high ductilities. The base stub was a 700 mm x 1800 mm rectangular steel block with a cylindrical cavity to hold the specimen. The space between the specimen and base was filled with a 15.9 mm thick layer of grout. Since the stub block had very high capacity compared to the specimen, it was assumed to be rigid with negligible deformations, and hence, the pile was assumed to be fixed at the base.

A 5000 kN loading jack was used to apply the vertical axial load. The lateral load was applied using two horizontal 2000 kN jacks in the east (positive drift) and west (negative drift) directions. All specimens were controlled by drift ratios, R_{test} (%) for two loading cycles of 0.25%, 0.5%, 0.75%, 1.0%, 1.5%, 2.0%, 3.0% and 5.0%.

Figure 2 shows the instrumentation comprising of several strain gauges and displacement gauges that were installed along the outer surface of the casing, in the vicinity of plastic hinge zones to measure the longitudinal strains and curvatures.

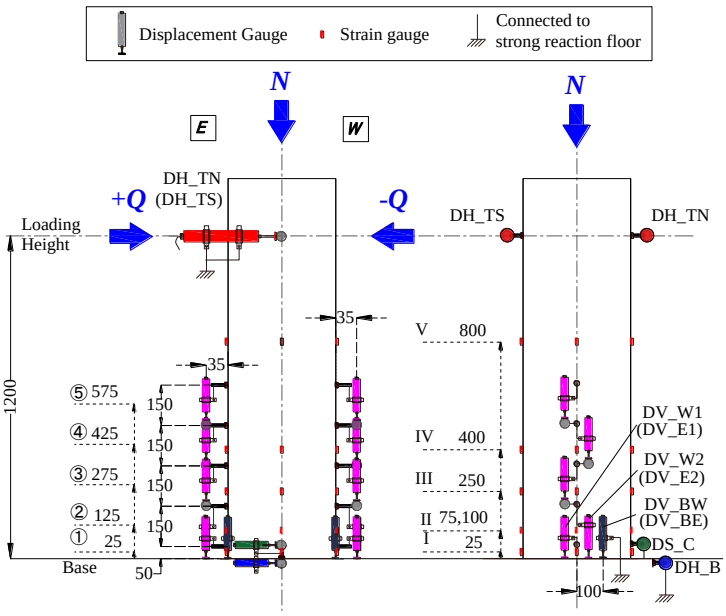

Figure 2: Measurement system (dimensions in mm)

Equations 1, 2, and **3** were used to calculate the drift, R, at top and moment, M_x, at any height, x, from the base. The additional bending moment due to P-Δ effect was also considered in the calculation of M_x. As shown in **Figure 3**, $\delta 1$ is the horizontal displacement of the free end; $\delta 2$ is the horizontal displacement of the stub; $\delta 3$ is the relative horizontal movement between the pile and the base stub; θ_b is the rotation

of the base; θ_{ul} is the rotation due to uplift of the pile from the stub and, δ_{DV_W1} and δ_{DV_E1} are the measurements from gauges DV_W1 and DV_E1, respectively, with a distance of 470 mm from each other. The lateral load, Q, and axial load, N, were measured by their corresponding load cells. For x = 25 mm and 75 mm, it is assumed that drift from the bottom is zero i.e., $\delta_{25} = \delta_{75} = 0$.

$$R = R_{test} - \theta_{ul} = \frac{\delta 1 - \delta 2 - \delta 3}{L} - \theta_b - \theta_{ul} \quad (1)$$

$$M_x = Q(L - x) + N(\delta 1 - \delta_x) \quad (2)$$

$$\theta_{ul} = \frac{\delta_{DV\_W1} - \delta_{DV\_E1}}{400 + 2 * 35} \quad (3)$$

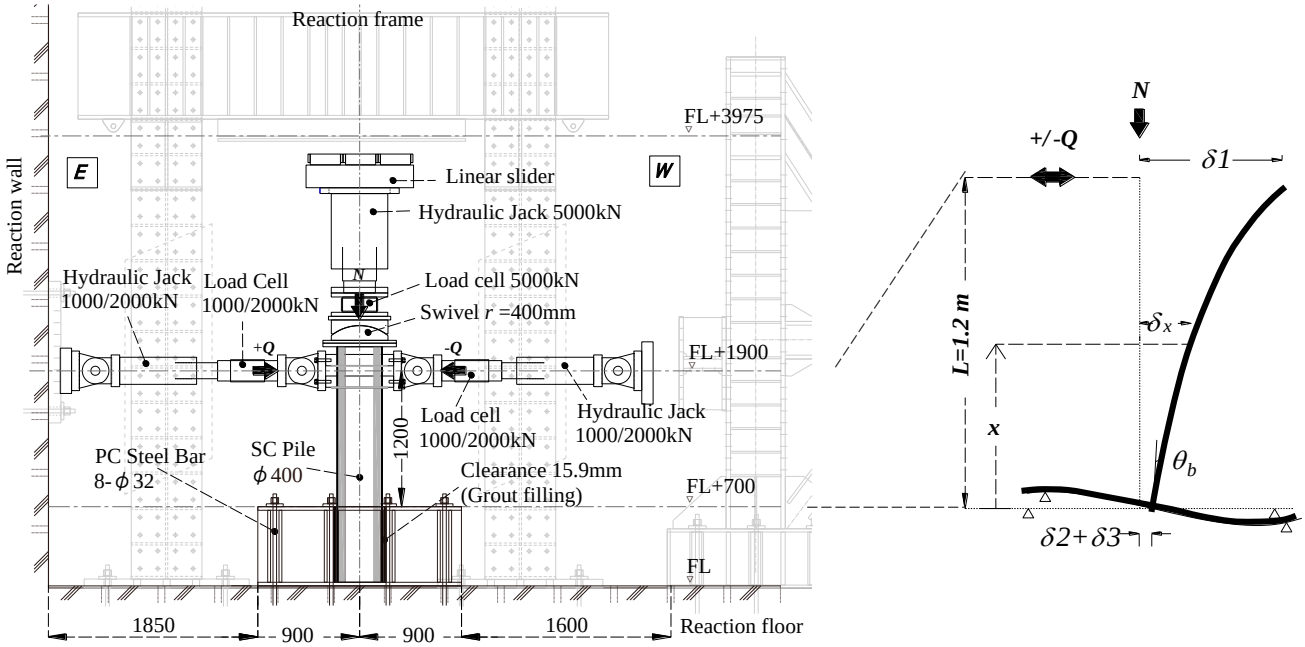

Figure 3: Schematic diagram of the test setup along with the simplified diagram of the deformations and rotations in the specimen.

3. Experimental results and discussion

3.1. General behavior

The moment-curvature responses of all test specimens are shown in **Figure 4**. The plots also mark the points on the curve corresponding to load steps where various characteristic events occurred i.e., yielding (compressive and tensile) of the extreme fiber of steel casing, the maximum moment at the base, $M_{0,max}$, and the ultimate moment M_u. The load step corresponding to the onset of buckling was identified by strength degradation and photographic evidence and is also marked on the curve. For this study, the ultimate point was defined by either 20% degradation of moment carrying capacity from the peak moment in the envelope curve or the maximum observed curvature. In the case of SC5 and SC6 piles, a sudden drop in strength, more than 20%, was observed after reaching the maximum moment capacity and hence the load step just before this drop was chosen as the ultimate point**. Table 2** summarizes the moments and their corresponding drifts and curvatures observed at points of maximum moment and ultimate moment for all piles. Here ϕ_y is defined as the curvature at either the tensile or compression yielding of steel casing, whichever was observed first.

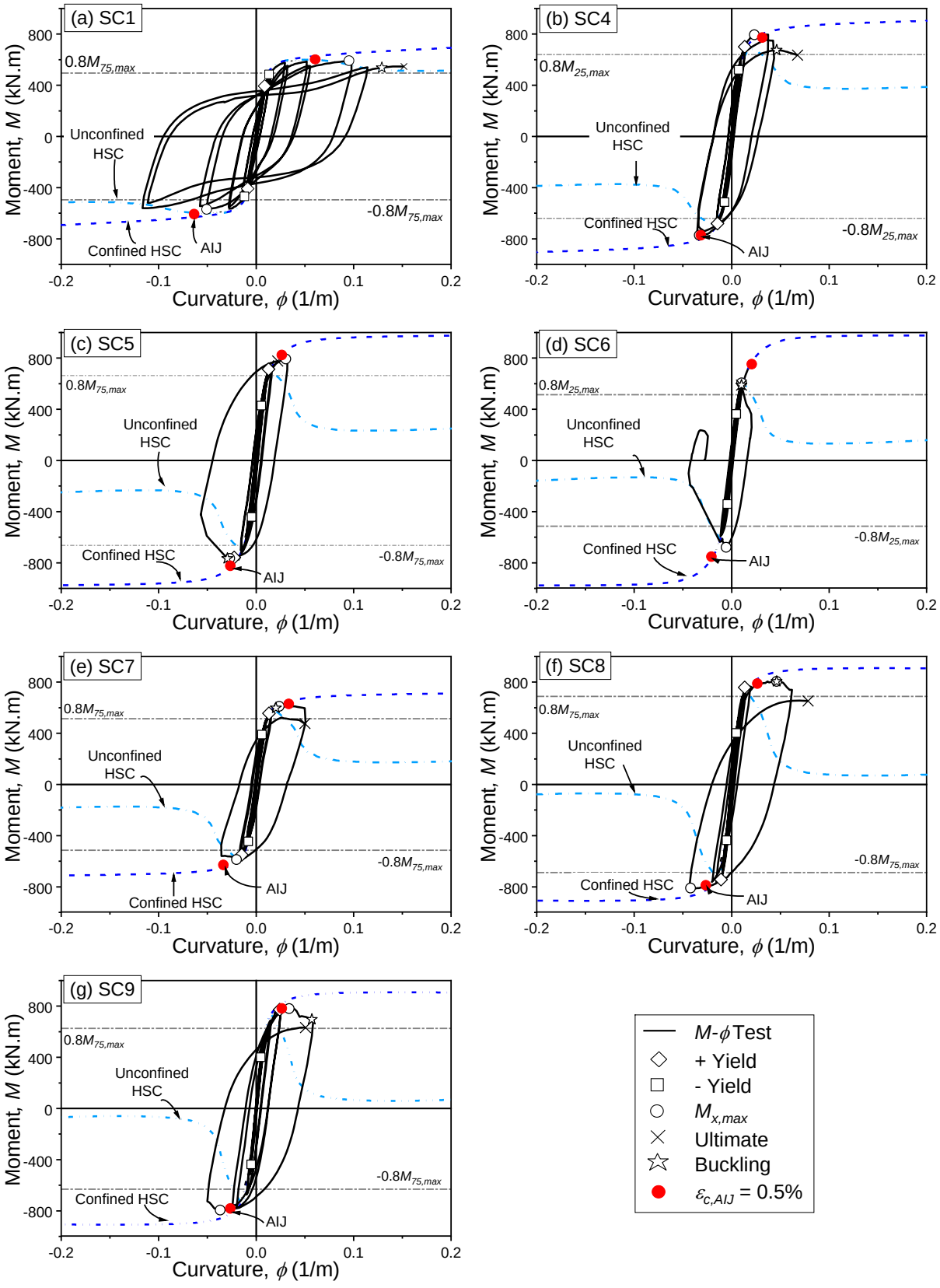

Figure 4: Cyclic moment-curvature response of piles along with results from theoretical analysis.

Table 2: Summary of maximum and ultimate moment, and corresponding drift ratios and curvatures. Average maximum load capacity is also shown.

Pile	Yield curvature ϕ_y	Maximum						Ultimate*			Average Load Q_{max}	Curvature ductility ϕ_u / ϕ_y	Initial stiffness EI
		ϕ at $M^+_{0,max}$	R at $M^+_{0,max}$	$M^+_{0,max}$	ϕ at $M^-_{0,max}$	R at $M^-_{0,max}$	$M^-_{0,max}$	ϕ_u	R_u	M_u			
	(1/m/10^2)	(1/m/10^2)	(%)	(kN.m)	(1/m/10^2)	(%)	(kN.m)	(1/m/10^2)	(%)	(kN.m)	(kN)		(MPa.m^4)
SC1	0.88	9.55	2.06	631	-5.08	-1.11	-608	15.17	-#	584	515	17.2	64.2
SC4	0.71	3.74	0.71	813	-3.32	-0.80	-789	6.77	0.72	647	638	9.5	81.4
SC5	0.54	3.22	0.73	845	-2.96	-0.78	-815	2.21	0.72	825	648	4.1	82.2
SC6	0.48	1.02	0.38	651	-0.56	-0.22	-724	1.02	0.47	636	547	2.1	81.2
SC7	0.61	2.07	0.65	639	-1.86	-0.62	-624	5.00	1.25	507	504	8.2	75.1
SC8	0.48	4.63	0.82	856	-4.22	-0.92	-865	7.84	1.10	691	669	16.3	85.6
SC9	0.49	3.39	0.44	830	-3.69	-1.08	-844	5.06	0.27	671	655	10.3	88.8

*Corresponds to data captured 1) at maximum drift for SC1, 2) before a sudden drop in the moment after reaching maximum capacity for SC4 and SC5, and 3) at a drop in the moment-carrying capacity by 20% for the rest.;
Not captured due to the removal of level ① displacement gauge.

It was observed that the moment and load-carrying capacities of axially loaded test specimens were influenced by the onset of local buckling of the steel casing in the later cycles. Specimens with higher compressive axial loads were stiffer at smaller drifts, but stiffness degraded abruptly with the development of local buckling. **Figure 5** shows the observed buckling at the end of the test for SC1 and SC5 piles. Buckling extended up to a length of around 100 mm in all cases. The buckling first occurred at one of the extreme compression fibers in either positive (west) or negative (east) direction, and then it spread along the circumference in case of piles with compressive axial loads. In the case of SC1 pile, there was some residual drift at the end of loading because permanent buckling occurred only in the negative direction (the last loading cycle was R_{test} = -5.0%) as seen in **Figure 5(a)**. After removal of steel casing at the end of loading, concrete under the region of buckling to a height of 125 mm (0.31*D*) was found to be crushed in all cases as shown in **Figure 6** and **Figure 7** for SC1 and SC5, respectively. As inferred by Park et al. 1983 **[3]** for similar damage, this region represents the zone of concentrated plastic damage.

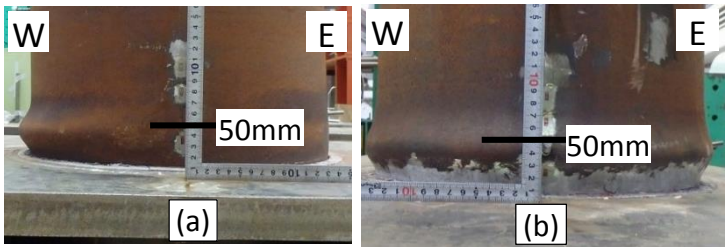

Figure 5: (a) SC1 and (b) SC5 piles at the end of loading

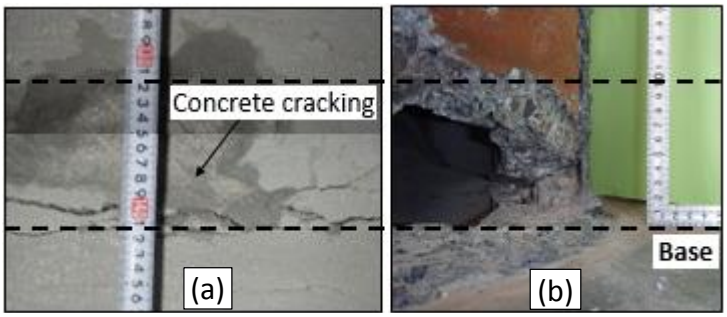

Figure 6: Zone of concentrated plastic damage in SC1 pile after (a) removal of the casing and (b) scrapping off concrete.

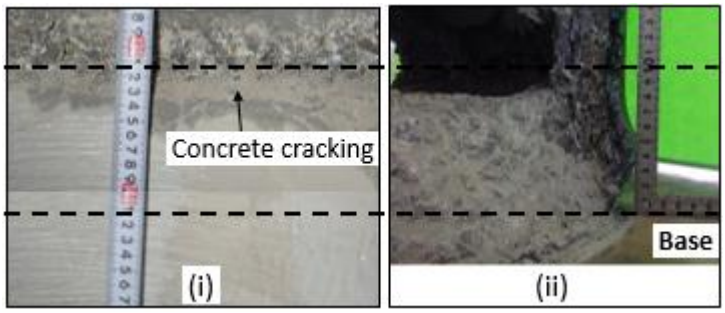

Figure 7: Zone of concentrated plastic damage in SC5 pile after (a) removal of the casing and (b) scrapping off concrete.

SC8 and SC9 piles with filling materials showed very different behavior from the hollow piles. These piles were more ductile and could sustain loads to comparatively higher drift levels at high axial load

ratios. The damaged region extended to 100 mm and crushing in filling material occurred at the same height as that of the concrete layer.

No fracturing of steel casing was seen in any of the current tests. By the end of loading, yield curvature, ϕ_y, was exceeded in over 528 mm to 600 mm height i.e. 0.44 L to 0.50 L.

3.2. Comparison of performance

In this section, performance is compared for piles with different axial load, with different thickness of casing, with different filling materials, and for piles with or without filling material. The performance is evaluated based on moment and load carrying capacity, strength degradation and curvature ductility. Curvature ductility is defined as the ratio ϕ_u / ϕ_y. **Figure 8** compares the capacity of five of the tested piles in terms of their curvature ductility and maximum moment capacity.

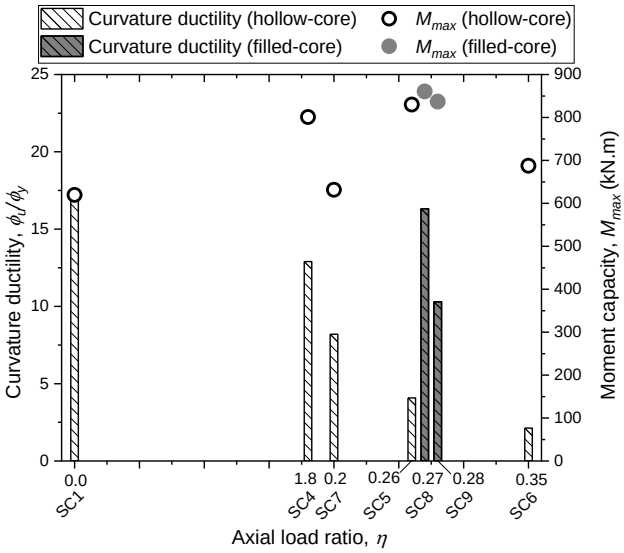

Figure 8: Curvature ductility and moment capacity of SC piles from experiment.

Piles with different compressive axial loads

Comparing moment-curvature behavior between SC1, SC4 and SC5 piles shows that increasing the axial load increases the initial stiffness as well as moment capacity of specimens as seen in **Table 2.** However, because of early onset of local buckling, axially loaded SC4 and SC5 piles showed sudden and early strength degradation. Curvature ductility of SC1 pile is 1.81 and 4.22 times greater than those of SC4 and SC5 piles, respectively. SC4 and SC5 piles showed stable behavior up to R_{test} = 1% (4th load cycle) and then started losing strength due to buckling of extreme compression fibers in the casing. On the other hand, SC1 pile remained stable up to R_{test} = 5% (8th load cycle) with no considerable decrease in moment capacity.

Piles with different thickness of casing

Comparing the performance of SC4 (t_s = 6 mm, f_y = 505 MPa, N = 2000 kN) and SC7 (t_s = 4.5 mm, f_y = 453 MPa, N = 2000 kN) piles shows that SC4 pile had a greater moment and load bearing capacity than SC7 pile both before and after yielding of casing. Reducing the steel to concrete strength ratio, $f_y A_s / f_c A_c$ by 35% from SC4 to SC7 resulted in decrease of $M_{0,\max}$ by about 22.0% and curvature ductility by 13.0%. However, the performance in terms of drift remained similar in both cases. More importantly, decreasing the casing thickness resulted in earlier buckling. Hence, buckling of casing rather than concrete crushing became the factor governing the moment capacity in SC7 pile while this was not the case for SC4 pile.

Piles with different filling material

The core of SC8 and SC9 piles were filled with cement paste and normal concrete, respectively. These materials have very different Young's modulus but the performance of SC8 and SC9 piles was almost identical. Concrete filling increased the maximum and ultimate bending moment capacities $M_{0,\max}$ and M_u by only 2.3% and 2.0%, respectively compared to cement paste filling. This shows that the

choice of filling has little effect on the strength. However, filling with either material contributes to improvement in the ductility performance by providing confinement to outer HSC, as will be seen in the next subsection.

Comparison of piles with filled core and hollow piles

Comparing core-filled piles with SC5 pile which had the same axial load ratio and less axial load shows that core-filled piles had more moment and load carrying capacity as well as ductility. In the case of SC5 pile, the largest drift to which the pile could be tested was R_{test} = 2% (6th load cycle), while in the case of both SC8 and SC9 piles the largest drift corresponded to R_{test} = 5% (8th load cycle). It can also be seen that in general core-filled piles with high axial loads are more ductile compared to hollow piles with same axial load. It is also worth noting that curvature ductility capacity of core filled piles with 3500 kN axial load (η = 0.27 and 0.28) is similar to SC1 pile that had no axial load (η = 0). It should be noted that while designing SC piles according to current design guidelines, the filling material properties are ignored, and the pile is assumed to be hollow. Comparing SC6 and SC8 pile in **Figure 8** it is clear that ignoring the effect of filling material would lead to very conservative design as core-filled SC8 pile had 1.2 times more moment carrying capacity and 7.7 times larger ultimate curvature than hollow SC6 pile.

The hysteretic behavior of core filled piles was markedly different from hollow piles because these piles retained some of their moment carrying capacity even after buckling. In both SC8 and SC9 piles it was observed that the capacity started decreasing in the R_{test} = 1% cycle temporarily but afterwards a slight increase in capacity was seen with increase of drift in both cases. The local buckling and crushing of spun HSC and filling material led to the large hysteric loops seen in the later cycles.

From the above discussion, it can be inferred that by prevention of concrete spalling on the inner side (i.e. by addition of filling material), a drift performance similar to the case of no axial load can be achieved even in case of high axial loads with $\eta \approx 0.3$. This shows the advantage that these core filled piles have over hollow piles in terms of strength and ductility. This is an economical solution, the benefit of which might be taken by choosing a low-cost material for core filling to ensure that the HSC layer is amply confined.

4. Section analysis using fiber-based models

4.1. Model Description

In order to assess the theoretical behavior of SC piles, monotonic moment-curvature analysis was carried out for the test sections using OpenSees. Apart from the basic assumptions that go with sectional analysis, other important assumptions with the model were: 1) no slip was assumed between concrete and steel casing, 2) buckling was not modelled and 3) in cases where confinement was modelled, the confinement coefficient, C_c, was calculated by using the model by Muguruma et al. **[4]**, assuming the steel spacing to be zero. Three concrete models were used for comparison. The stress-strain curves for the three concrete models are shown in **Figure 9** along with the curve from the material test. The stress-strain curves for the steel models are shown in **Figure 10.**

AIJ model:

The first model is an elastic-perfectly plastic (bilinear) model based on AIJ guidelines **[5]** for design of hollow SC piles. The guidelines stipulate to assume the concrete to be unconfined with an ultimate strain value of 0.5% beyond which the concrete is assumed to take no further stress. Hence, the capacity of pile at this point is the ultimate capacity. Also, concrete is assumed to have no tensile strength. An elastic-perfectly plastic model was also used for steel casing per AIJ guidelines **[5]**.

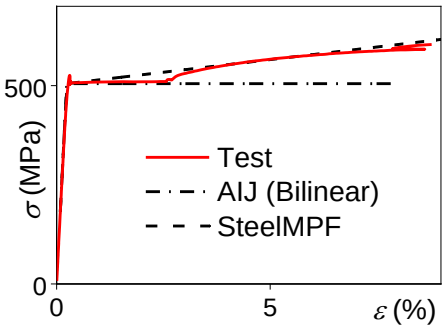

Figure 9: Stress-strain envelop of steel

Lower and upper bound models:

Owing to a lack of clear data on confinement effect in circular hollow SC sections filled with HSC, a lower bound and upper bound approach similar to Park et al. **[3]** was adopted. The upper bound approach assumed full composite action and confinement in concrete with C_c calculated from **Eq. 4**. Because of the unknown bond behavior between casing and concrete and unknown dilatancy parameters to model confinement in HSC, the lower bound approach assumed the case of no confinement in concrete. The unconfined plain concrete was modeled using the Muguruma model (Muguruma et al. **[4]**) for high strength concrete in circular section. Strain at compressive strength of plain concrete, ε_m , was taken from the material test data whereas the strain at ultimate strength, ε_u, was determined using **Eq. 5**. For confined concrete, the model proposed by Komuro et al. **[6]** was used which is based on modified Muguruma model **[4,7]** for confined high strength concrete. The parameters for confined high strength concrete i.e. strain at compressive strength of confined concrete, ε_{cm}, maximum compressive strength, σ_{cm}, and strain at ultimate strength of confined concrete, ε_{cu}, were calculated according to **Equations 6, 7** and **8**. These models were implemented in OpenSees by changing the compression side envelope curve in *Concrete02* (OpenSees) uniaxial material. Concrete strength in tension, f_t, was taken as 0.14 f_c and tension softening stiffness was taken as f_t/0.002.

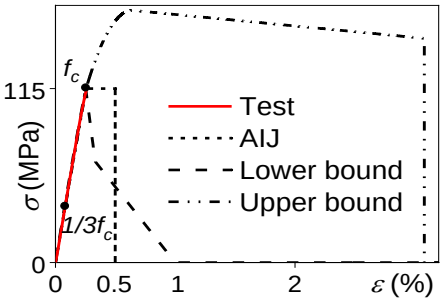

Figure 10: Stress-strain envelope of concrete

$$\varepsilon_u = 1.314\varepsilon_m \quad (5)$$

$$\varepsilon_{cm} = (1 + 250C_c)\varepsilon_m \quad (6)$$

$$\sigma_{cm} = (1 + 75C_c)f_c \quad (7)$$

$$\varepsilon_{cu} = (0.401 + 1460C_c)\varepsilon_u \quad (8)$$

In both upper and lower bound cases, steel was modelled using *SteelMPF* (OpenSees) uniaxial material, which represents constitutive nonlinear hysteretic material model for steel proposed by Menegotto and Pinto **[8]** and extended by Filippou et al. **[9]** to include isotropic strain hardening effects.

The model using unconfined Muguruma model for concrete and *SteelMPF* material model for steel is henceforth denoted as the lower bound model while the model using confined Muguruma model for concrete and *SteelMPF* material model for steel is henceforth denoted as the upper bound model. The maximum moment capacities of all piles is expected to lie within these bounds.

4.2. Comparative evaluation of numerical models

Table 3 gives a comparison of flexural strength from test to the calculated values. In the case of the AIJ model, the moment capacity when strain in concrete is 0.5% has been used for comparison and is denoted by $\varepsilon_{c,AIJ}$ = 0.5%.

Figure 4 shows the moment vs curvature relationship generated from these numerical models.

It is seen that the AIJ model gives very reliable prediction of moment capacity based on $\varepsilon_{c,AIJ}$ = 0.5% value with only ±9% error. This model might be used for prediction of design strength for piles with low axial load ratio. As the axial load ratio increases to more than 0.26, the moment capacity seems to depend more on buckling of steel casing than on concrete crushing which makes this model ineffective. In addition to this, owing to its simplicity, this model cannot be used for simulation of hysteretic behavior of piles.

Table 3: Comparison of maximum moment. Ratio of experimental to theoretical values are shown for the three theoretical models.

Model	AIJ	Lower bound	Upper bound
Pile			
SC1	1.02	1.03	0.89
SC4	1.04	1.17	0.89
SC5	1.01	1.18	0.85
SC6	0.91	1.11	0.70
SC7	0.98	1.10	0.89
SC8	1.09	1.21	0.95
SC9	1.07	1.15	0.92
Average	1.02	1.14	0.87

As expected, the upper and lower bounds were able to bracket the moment capacities from tests within their limits for all piles. The lower bound model showed degradation in strength due to crushing of the unconfined concrete before reaching the maximum capacity from test, whereas the upper bound model overestimated the test capacity by overshooting the values after buckling was observed in the test for hollow axially loaded piles. In the case of core filled piles, the confined HSC model was able to give a good prediction of maximum moment capacity implying that the assumption of full confinement of concrete is correct for filled-core piles. The capacity degradation after buckling could not be simulated well.

Buckling rather than concrete crushing tends to govern strength degradation in hollow piles with high axial loads. On the other hand, in the case of SC1 pile with no axial load, concrete crushing tends to govern the strength degradation as can be seen from capacity drop in the curve from the lower bound model after reaching maximum capacity. This shows that the criteria governing maximum capacity of SC piles shifts from concrete crushing to buckling as the axial load increases. However, it is difficult to establish the degree of confinement in hollow piles from the results of seven specimens. Theoretical strength calculations for both maximum and ultimate capacities became unreliable in the case of hollow SC piles with $\eta > 0.26$ because buckling preceded the occurrence of theoretical maximum strength.

5. Conclusions

An experimental study was conducted on seven hollow steel-encased concrete (SC) piles made with high strength concrete (HSC) to examine the effects of high axial loads, concrete thickness, steel casing thickness and filling material on their performance under cyclic loading. The tests were conducted on 400 mm diameter sections made of HSC of grade 105 MPa under applied axial load ratio in the range of 0~0.35. A comparison with theoretically obtained moment capacity was also conducted by section analysis in OpenSees using 1) elastic perfectly plastic models for steel and concrete, and 2) unconfined and 3) confined Muguruma models for HSC with a modified Menegotto-Pinto model for steel. Attention was paid particularly to the ultimate behavior, maximum moment capacity and ultimate curvature. Based on the results of this experimental investigation, the following conclusions are drawn:

1) The moment and load-carrying capacity of hollow, axially loaded piles with $\eta \geq 0.26$ were influenced by the onset of buckling which caused the strength to decrease abruptly. It was seen that for $R_{test} < 1.5\%$, most curvature deformations were concentrated between 0 mm to 125 mm ($0.31D$) height.
2) On comparing the behavior of SC4 and SC7 piles, it was observed that reducing the steel to concrete ratio, $f_y A_s / f_c A_c$, by 35% resulted in a decrease in $M_{0,\max}$ by about 22% and curvature ductility by 14.0%. Additionally, buckling of casing rather than concrete crushing became the factor governing the moment capacity in the SC7 pile with thinner casing.
3) The addition of filling material dramatically improved the ductility of piles by prevention of spalling of inner concrete. The hysteretic behavior of core-filled piles included retention of moment carrying capacity even after buckling of steel casing. Further, a drift performance similar to the case of hollow piles with no axial load could be achieved in core-filled piles with high axial loads of 3000 kN.
4) A comparison with theoretical observations showed that strength degradation in these piles is caused either by concrete crushing or buckling. Concrete crushing is the governing factor for hollow SC piles loaded with a low compressive axial load while the factor shifts to buckling as the axial load is increased. Theoretical strength calculations for both maximum and ultimate capacities became unreliable for hollow SC piles with $\eta \geq 0.26$ because buckling preceded the occurrence of theoretical maximum strength.

6. Acknowledgements

This work was supported financially by JSPS through two Grant-in-Aid programs (PI: Shuji Tamura, and Susumu Kono). We are thankful to the Concrete Pile and Pole Industrial Technology Association and Steel encased Cast-in-place Concrete Piles Association for their expert advice and support. We are also thankful to the Consortium for Socio-Functional Continuity Technology (PI: S. Yamada), the Collaborative Research Project (Materials and Structures Laboratory), the World Research Hub Initiative (Institute of Innovative Research), at Tokyo Institute of Technology, and Ministry of Education, Culture, Sports, Science and Technology (MEXT), Japan for their generous support of this work.

7. References

[1] Tokimatsu K, Asaka Y. Effects of liquefaction-induced displacements on pile performance in the 1995 Hyogoken-Nambu earthquake. Spec Issue Soils Found 1998:163–77.
[2] Horikoshi K, Tateishi A, Ohtsu H. Detailed Investigation of Piles Damaged By Hyogoken-Nanbu Earthquake. 12th World Conf. Earthq. Eng., Auckland, New Zealand: 2000, p. CD-ROM, Paper No. 2447.
[3] Park RJT, Priestley MJN, Walpole WR. The Seismic Performance of Steel Encased Reinforced Concrete Bridge Piles. Bull New Zeal Natl Soc Earthq Eng 1983;16:123–40.
[4] Muguruma H, Watanabe F, Iwashimizu T, Mitsue R. Study on improving the ductility of high-strength concrete by lateral confining [In Japanese]. JCI, Proc. 5th Annu. Conf., 1983, p. Vol. 5, 317-320.
[5] Architectural Institute of Japan. Guidelines for performance evaluation of earthquake resistant reinforced concrete buildings (Draft) [In Japanese]. 2004.
[6] Komuro T, Imai K, Muramatsu A, Korenaga T, Watanabe F. Compressive properties of reinforced concrete columns using high strength concrete with compressive strength of 100-180N/mm^2 [In Japanese]. J Struct Constr Eng (Transactions AIJ) 2004;69:77–84.
[7] Watanabe F, Nishiyama M, Muguruma H. Strength and ductility of ultra high strength concrete column [In Japanese]. J Struct Constr Eng (Transactions AIJ) 1993;446:99–106. doi:10.3130/aijsx.446.0_99.
[8] Menegotto M, Pinto PE. Method of Analysis for Cyclically Loaded R. C. Plane Frames Including Changes in Geometry and Non-Elastic Behavior of Elements under Combined Normal Force and Bending. Proc IABSE Symp Resist Ultim Deform Struct Acted by Well Defin Loads 1973:15–22.
[9] Filippou FC, Popov EP, Bertero VV. Effects of Bond Deterioration on Hysteretic Behaviour of Reinforced Concrete Joints. Report to the National Science Foundation. California: 1983.

